Journal of Computational and Applied Mathematics 457 (2025) 116273

Contents lists available at ScienceDirect

Journal of Computational and Applied Mathematics

journal homepage: www.elsevier.com/locate/cam

Positivity preserving and unconditionally stable numerical scheme for the three-dimensional modified Fisher–Kolmogorov–Petrovsky–Piskunov equation

Seungyoon Kang, Soobin Kwak, Youngjin Hwang, Junseok Kim *

Department of Mathematics, Korea University, Seoul 02841, Republic of Korea

ARTICLE INFO

Keywords:
Fisher–Kolmogorov–Petrovsky–Piskunov equation
Unconditionally stable method
Positivity preserving scheme
Operator splitting method

ABSTRACT

This paper introduces a numerical approach for the practical solution of the modified Fisher–Kolmogorov–Petrovsky–Piskunov equation that describes population dynamics. The diffusion term and nonlinear term is based on the operator splitting method and interpolation method, respectively. The analytic proof of the discrete maximum principle and positivity preserving for the numerical algorithm is demonstrated. Numerical solution calculated using the proposed method remains stable without blowing up, which implies that the proposed method is unconditionally stable. Numerical studies show that the proposed method is second-order convergence in space and first-order convergence in time. The performance and applicability of the proposed scheme are studied through various computational tests that present the effects of model parameters and evolution dynamics.

1. Introduction

The dynamics of population genetics and wave propagations can be explained by a simple, but realistic model by Fisher [1] which exhibits a traveling wave solution. Another pioneering work by Kolmogorov, Petrovsky and Piskunov [2] studied a more general equation with reaction term

$$u_t = \Delta u + f(u),\ 0 < u < 1, \tag{1}$$

where f is a smooth function that satisfies $f(0) = f(1) = 0,\ f'(u) > 0$ for $0 < u < 1,\ f'(0) = \alpha > 0$ and $f'(u) < \alpha$ for $0 < u \leq 1$. Kolmogorov et al. discussed the traveling wave solution and provided a general approach using $f = Ku(1-u)^2$. After the classic works of Fisher and Kolmogorov et al. there are many significant contributions on modification of the Fisher–Kolmogorov–Petrovsky–Piskunov (Fisher–KPP) equation due to extensive applications in chemistry and biology. One example is the non-local Fisher–KPP equation, where it models non-local interaction and competition [3]. Variable x interprets a morphological trait, the diffusion term models mutation and modified nonlinear term mimics competition [4]. Berestycki et al. [5] defined a non-local saturation effect defined through an given convolution kernel and applied the Fisher–KPP equation, which can model saturation or competition effects. The authors proved the existence of steady states and traveling waves. Therefore, the proposed equation admits traveling wave solutions. Hamel and Henderson [6] investigated the influence of general non-local advection term to propagation in the one-dimensional Fisher–KPP equation. This model is a generalization of the Keller–Segel–Fisher system. Achleitner and Kuehn [7]

* Corresponding author.
E-mail address: cfdkim@korea.ac.kr (J. Kim).
URL: https://mathematicians.korea.ac.kr/cfdkim (J. Kim).

https://doi.org/10.1016/j.cam.2024.116273
Received 19 March 2024; Received in revised form 12 August 2024
Available online 10 September 2024

proposed an analysis of stationary solutions for the non-local Fisher–KPP equation. The authors expect that results of this paper can be generalized to obtain solutions of other non-local evolution equations. Shapovalov et al. [8] described the evolution of spatiotemporal structures depending on the equation parameter domain using the non-local Fisher–KPP equation. The paper also presents the effect of relaxation on the pattern formation in a non-local population model.

While studies concerning the non-local Fisher–KPP equation modified the nonlinear term, Audrito and Vázquez [9] studied a doubly nonlinear Fisher–KPP equation where they replaced the diffusion term as $\Delta_p u^m$ where Δ_p is the $p-$Laplacian defined as $\Delta_p v := \nabla \cdot (|\nabla v|^{p-2}\nabla v)$ with parameters $m > 0$ and $p > 1$. Fisher–KPP equation is also studied by Xu et al. [10], with the birth and death function as the nonlinear equation and time delayed degenerate diffusion equation. The governing equation also has a traveling wave solution like the Fisher–KPP equation, but shows a critical sharp pattern. The existence, uniqueness and regularity of the traveling wave is demonstrated. Like this, generalized Fisher–KPP equations are proposed by replacing constant parameters and variable functions for prominent applications in ecology, physiology, combustion, crystallization, plasma physics, and phase transition problems [11]. Wang et al. [12] studied the global stabilization of solutions to initial–boundary value problems of the generalized Fisher–KPP equation. The applicability of the proposed method is shown by comparing the results obtained from the diffusive susceptible–infected–susceptible model. In [13], the authors studied the positivity of solutions to the Fisher–KPP equation with relaxation time included. Both analytical and numerical results are presented in the paper. An energy analysis of the generalized theory is given and the existence of a threshold for the relaxation time is shown numerically. Gilding and Kersner [14] presented a generalization of Fisher–KPP equation that embodies other well-known reaction–convection–diffusion equations:

$$u_t = (u^m)_{xx} + (u(b_0 + b_1 u^p))_x + \begin{cases} u^{2-m}(1-u^p)(c_0 + c_1 u^p) & \text{for } u > 0, \\ 0 & \text{for } u = 0, \end{cases} \tag{2}$$

where the classic Fisher–KPP equation can be obtained from $m = p = c_0 = 1$ and $b_0 = b_1 = c_1 = 0$. Let us mention that the Newell–Whitehead–Segel equation [15], FitzHugh–Nagumo model [16,17] and Burgers equation [18] can be found by applying different parameter values at Eq. (2).

Three- and multi-dimension Fisher–KPP equation is also a popular topic. One might recall this kind of approach from the pioneering works of the Fisher–KPP equation. While Fisher [1] studied a 1D classic Fisher equation, Kolmogorov, Petrovsky and Piskunov [2] studied a more general equation in 2D. Gärtner [19] studied the traveling wave front in high dimension Fisher–KPP equation and showed that the transition has a width that is uniformly bounded in time. Ducrot [20] also studied asymptotic behavior in an asymptotic homogeneous medium at multi-dimension case. Prior to the convergence study, a precise estimate of the location was found. The authors found that the location depends on the rate of medium reaching infinity. Relation between the rate of convergence and location is also demonstrated. Du and Ni [21] studied the high-dimensional symmetric Fisher–KPP equation with non-local diffusion and free boundary. Authors focused on the long time dynamics of the proposed model. In the first study, the threshold condition of the kernel function and spreading speed in finite time were demonstrated. Some specific domains such as a cone in $\mathbb{R}^N$ can be selected as a domain for the high-dimensional Fisher–KPP equation, studied by Lou and Lu [22]. They adopted the Dirichlet boundary condition and demonstrated the unique convergence of the spreading phenomena. They concluded that the spreading speed depends on the propagation direction and boundary conditions, and not the shape of the cone. Vyas et al. [23] studied the neural population dynamics to demonstrate how they are computed and implemented. To describe dynamics in 3D and high-dimensional data, they introduced linear subspace, null space and manifold. Al-Musawi and Harfash [24] studied the extended Fisher–KPP equation on open bounded convex domains with dimensions 1 to 3. The semi-discrete and fully discrete finite element approximation is proposed to solve the governing equation. Proof of the existence and uniqueness of solutions and various numerical experiments support the proposed methods. Garvey et al. [25] presented a high-throughput platform for studying heterogeneous cell platforms. The authors mentioned that for a realistic study on tumor cell populations, a 3D culture can be applied. The mathematical modeling of multi-dimensional population dynamics using the Fisher–KPP equation has been a popular subject for the past decades [26]. The Fisher–KPP equation has been applied in various population genetic studies such as cell growth through cell communication and aggregation [27], spreading of biological or chemical species [28] and spreading nature of invasive species [29].

The paper is organized as follows. The governing equation is given in Section 2. In Section 3, we describe the proposed computational method for the 3D Fisher–KPP equation. In Section 4, numerical analyses are given. We conducted computational tests to validate the robustness of the proposed method in Section 5. In Section 6, we draw a conclusion. Additionally, detail operator splitting method (OSM) algorithm and pseudo code of the complete numerical algorithm is given in Appendices A and B, respectively.

2. Governing equation

This paper is devoted to the numerical method for the 3D modified Fisher–KPP equation that satisfies the discrete maximal principle, positivity-preserving and unconditionally stable.

$$\frac{\partial u(x,y,z,t)}{\partial t} = D\Delta u(x,y,z,t) + K_{pq} u^p(x,y,z,t)[1-u(x,y,z,t)]^q, \quad (x,y,z) \in \Omega. \tag{3}$$

$u(x,y,z,t)$ stands for the density of the population at time t and spatial location (x,y,z), defined on domain Ω. Note that the governing equation can be obtained from the general Fisher–KPP equation given in Eq. (2).

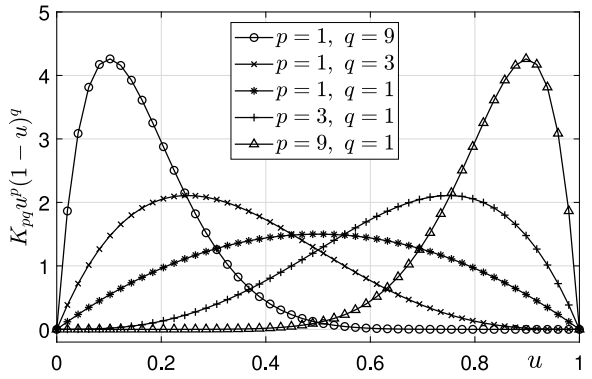

Fig. 1. $K_{pq}u^p(1-u)^q$ depending on values of p and q.

Diffusion coefficient D, nonlinear parameter K_{pq} and order of nonlinear terms p, q are all positive parameters. The nonlinear term $K_{pq}u^p(1-u)^q$ depends on the values of p and q. However, it must satisfy the following to clearly compare the parameter effects.

$$\int_0^1 K_{pq}u^p(1-u)^q du = 1. \tag{4}$$

Therefore, the nonlinear parameter K_{pq} varies according to the order of nonlinear terms like the following:

$$K_{pq} = \frac{\Gamma(p+q+2)}{\Gamma(p+1)\Gamma(q+1)} \text{ and } \Gamma(z) = \int_0^\infty t^{z-1}e^{-t}dt, \tag{5}$$

which is also given in Fig. 1 and will be used for the entirety of this study.

One consideration of the modified Fisher–KPP equation is that it turns into a numerically stiff problem when the orders of nonlinear terms p and q are large. Adopting OSM [30] allows the proposed method to show stable results when dealing with high order nonlinear terms and solving the stiffness problem. Even though the governing equation is in 3D space, OSM allows simple and fast numerical computation. Furthermore, unconditional stability and positivity preserving can be achieved more easily by OSM [31–33]. These aforementioned properties are the main advantages of the proposed method.

3. Numerical solution

To numerically solve Eq. (3), we set a $N_x \times N_y \times N_z$ grid $\Omega = (L_x, R_x)\times(L_y, R_y)\times(L_z, R_z)$ in the 3D space. Let Δt be the time step, $h = (R_x - L_x)/N_x = (R_y - L_y)/N_y = (R_z - L_z)/N_z$ be the space step, and $\{(x_i, y_j, z_k) = (L_x + (i-0.5)h, L_y + (j-0.5)h, L_z + (k-0.5)h) | 1 \le i \le N_x, 1 \le j \le N_y, 1 \le k \le N_z\}$ be the set of cell centers. On these cell centers, we denote the numerical approximation $u(x_i, y_j, z_k, t_n)$ by u^n_{ijk} where $t_n = n\Delta t$. On the cell centered grid, the governing Eq. (3) is divided by the OSM in the following way:

$$u^{n+1}_{ijk} = (\mathcal{N}_{OSM} \circ \mathcal{L}^z_{OSM} \circ \mathcal{L}^y_{OSM} \circ \mathcal{L}^x_{OSM}) u^n_{ijk}. \tag{6}$$

Separating the governing equation into different physical processes can achieve simple and efficient numerical computation. Three discrete linear operators $\mathcal{L}^x_{OSM}, \mathcal{L}^y_{OSM}$ and $\mathcal{L}^z_{OSM}$ maps u^n_{ijk} to u^*_{ijk}, u^*_{ijk} to u^{**}_{ijk} and u^{**}_{ijk} to u^{***}_{ijk} using the following procedures, respectively:

$$\frac{u^*_{ijk} - u^n_{ijk}}{\Delta t} = D\frac{u^*_{i+1,j,k} - 2u^*_{ijk} + u^*_{i-1,j,k}}{h^2}, \tag{7}$$

$$\frac{u^{**}_{ijk} - u^*_{ijk}}{\Delta t} = D\frac{u^{**}_{i,j+1,k} - 2u^{**}_{ijk} + u^{**}_{i,j-1,k}}{h^2}, \tag{8}$$

$$\frac{u^{***}_{ijk} - u^{**}_{ijk}}{\Delta t} = D\frac{u^{***}_{i,j,k+1} - 2u^{***}_{ijk} + u^{***}_{i,j,k-1}}{h^2}. \tag{9}$$

Here, we used the one-dimensional discrete Laplacian operator [34]. Lastly, the nonlinear operator $\mathcal{N}_{OSM}$ maps u^{***}_{ijk} to u^{n+1}_{ijk} using an interpolation method that is discussed later. Combination of discrete linear operators $\mathcal{L}^z_{OSM} \circ \mathcal{L}^y_{OSM} \circ \mathcal{L}^x_{OSM}$ is a discrete solution for

$$\frac{\partial u(x,y,z,t)}{\partial t} = D\Delta u(x,y,z,t), \tag{10}$$

and the nonlinear operator $\mathcal{N}_{OSM}$ is a solution for

$$\frac{\partial u(x,y,z,t)}{\partial t} = K_{pq}u^p(x,y,z,t)[1 - u(x,y,z,t)]^q. \tag{11}$$

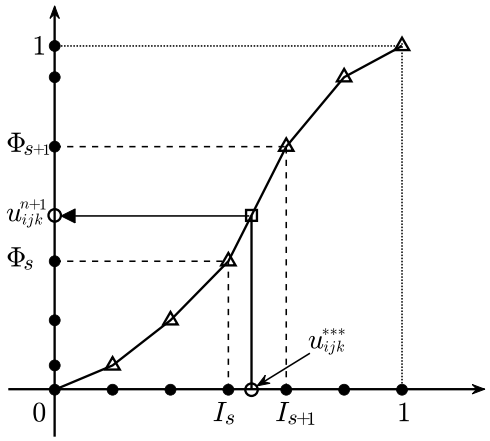

Fig. 2. Interpolation method for solving the nonlinear term.

When expressing Eqs. (7), (8) and (9) in an implicit form, we obtain a tridiagonal system for index i, j and k, respectively. Each tridiagonal system is solved using the Thomas algorithm [35]. We describe the detailed algorithm for solving Eqs. (7)–(9) in Appendix A. Now that we have solved the diffusion equation using the OSM method, the nonlinear reaction equation remains unsolved. We discretize Eq. (11) for a numerical solution. Numerical solution of the nonlinear reaction equation is unstable unless an exceptionally small time step is applied, especially with high p and q values. Therefore, the nonlinear operator $\mathcal{N}_{OSM}$ is defined using an interpolation method for a stable numerical solution. The basic concept of the novel interpolation method is to pre-compute accurate numerical solutions for the partial differential equation. Then, linear interpolation is applied based on the pre-computed values to obtain the desired numerical solution for each time step. Pre-computation is performed with N_τ times smaller time step $\Delta\tau$ to achieve high accuracy on pre-computing mesh $I = \{I_s | I_s = (s-1)/(M-1),\ \text{for}\ \ s = 1, \dots, M\}$. For given Δt, let $\boldsymbol{\Phi}_1, \dots, \boldsymbol{\Phi}_M$ be the corresponding pre-computed values in $[0,\ 1]$. To achieve stability, the following must be guaranteed so that pre-computed values are bounded by $[0,\ 1]$:

$$N_\tau = \begin{cases} \lfloor \Delta t K_{pq} \rfloor + 1 & \text{if } q = 1, \\ \lfloor \Delta t \left(\frac{p}{p+q-1}\right)^p \left(\frac{q-1}{p+q-1}\right)^{q-1} K_{pq} \rfloor + 1 & \text{if } q > 1, \end{cases} \tag{12}$$

where $\lfloor x \rfloor$ is the floor function. See [36] for pre-computed solutions $\boldsymbol{\Phi}$ on mesh I. Therefore, the nonlinear operator $\mathcal{N}_{OSM}$ maps u^{***} to u^{n+1} using the pre-computed solution.

$$u_{ijk}^{n+1} = \frac{I_{s+1} - u_{ijk}^{***}}{I_{s+1} - I_s} \boldsymbol{\Phi}_s + \frac{u_{ijk}^{***} - I_s}{I_{s+1} - I_s} \boldsymbol{\Phi}_{s+1}, \tag{13}$$

where $I_s \le u_{ijk}^{***} \le I_{s+1}$ for some s.

The schematic illustration of interpolation method is given in Fig. 2. We provided a pseudo code of the complete numerical algorithm in Appendix B.

Additionally, the discrete total mass of the numerical solution is defined in the following way [37]:

$$M = h^3 \sum_{k=1}^{N_z} \sum_{j=1}^{N_y} \sum_{i=1}^{N_x} u_{ijk}^n.$$

The total mass calculation plays an important role in discussing the effect of different parameter values.

4. Numerical analysis

The Fisher–KPP equation appears in the investigation of many realistic models, including the dynamics of the population. When the discrete variable u_{ijk} represents the density of the population at a desired position, the requirement of boundedness of the solutions is a significant physical condition that must be discussed [38,39]. In this section, we show the discrete maximum principle and positivity preserving of numerical solutions to observe the boundedness of the proposed method.

4.1. The discrete maximum principle

The first step of showing the boundedness of the proposed method starts with showing the discrete maximum principle. That is, the maximum component of each time step in the numerical method is bounded above by a maximum component [40]. We define the following notation that indicates the maximum value at some time step n.

$$\|u^n\|_\infty = \max u_{ijk}^n. \tag{14}$$

$\|u^*\|_\infty$, $\|u^{**}\|_\infty$ and $\|u^{***}\|_\infty$ is also defined as the maximum value of corresponding step. We will inductively show that the maximum value for each time step is monotonic decreasing. Therefore, we assume that the discrete maximum principle holds for initial condition and time step n with upper bound 1. First, we apply the triangle inequality to Eq. (26).

$$\begin{aligned}\left|\left(\frac{1}{\Delta t}+\frac{2D}{h^2}\right)u^*_{ijk}\right| &= \left|\frac{D}{h^2}u^*_{i-1,jk}+\frac{D}{h^2}u^*_{i+1,jk}+\frac{u^n_{ijk}}{\Delta t}\right| \\ &\le \left|\frac{D}{h^2}u^*_{i-1,jk}\right|+\left|\frac{D}{h^2}u^*_{i+1,jk}\right|+\left|\frac{u^n_{ijk}}{\Delta t}\right| \\ &\le \frac{D}{h^2}\|u^*\|_\infty+\frac{D}{h^2}\|u^*\|_\infty+\frac{1}{\Delta t}|u^n_{ijk}|. \end{aligned} \tag{15}$$

Eq. (15) holds for all i, j and k, which implies that $|u^*_{ijk}|$ on the left hand side can be replaced by $\|u^*\|_\infty$.

$$\begin{aligned}\left(\frac{1}{\Delta t}+\frac{2D}{h^2}\right)\|u^*\|_\infty &\le \frac{D}{h^2}\|u^*\|_\infty+\frac{D}{h^2}\|u^*\|_\infty+\frac{1}{\Delta t}\|u^n\|_\infty, \\ \|u^*\|_\infty &\le \|u^n\|_\infty. \end{aligned}$$

Then, $\|u^{**}\|_\infty \le \|u^*\|_\infty$ and $\|u^{***}\|_\infty \le \|u^{**}\|_\infty$ can be proved similarly. Lastly, we show that u^{n+1}_{ijk} is bounded by 1. Recall that index s satisfies $I_s \le u^{***}_{ijk} \le I_{s+1}$ and Φ_s and Φ_{s+1} are bounded by [0, 1], we obtain the following from Eq. (13).

$$u^{n+1}_{ijk} = \frac{I_{s+1}-u^{***}_{ijk}}{I_{s+1}-I_s}\Phi_s+\frac{u^{***}_{ijk}-I_s}{I_{s+1}-I_s}\Phi_{s+1} \le \frac{I_{s+1}-u^{***}_{ijk}}{I_{s+1}-I_s}+\frac{u^{***}_{ijk}-I_s}{I_{s+1}-I_s}=1.$$

We have shown that if the discrete maximum principle holds for time step n, it also holds for time step $n+1$. Inductively, the proposed method satisfies the discrete maximum principle.

4.2. Positivity preserving

In this section, we prove the positivity preserving of the proposed method. Continued from the last section, this will conclude the boundedness of the numerical scheme for the Fisher–KPP equation. Mathematical induction is also applied for this section. Assume that positivity preserving holds until time step n and the initial condition is positive. Let u^*_{IJK} be the minimum value of the numerical solution of the x-direction OSM for the linear equation

$$-\frac{D}{h^2}u^*_{i-1,jk}+\left(\frac{1}{\Delta t}+\frac{2D}{h^2}\right)u^*_{ijk}-\frac{D}{h^2}u^*_{i+1,jk}=\frac{u^n_{ijk}}{\Delta t}, \tag{16}$$

where I, J and K are indices of the minimum solution on the computational grid. When $2 \le I \le N_x - 1$, Eq. (16) at the minimum solution is given as following:

$$\begin{aligned}-\frac{D}{h^2}u^*_{I-1,JK}+\left(\frac{1}{\Delta t}+\frac{2D}{h^2}\right)u^*_{IJK}-\frac{D}{h^2}u^*_{I+1,JK} &= \frac{u^n_{IJK}}{\Delta t}, \\ \frac{1}{\Delta t}u^*_{IJK}-\frac{u^n_{IJK}}{\Delta t} &= \frac{D}{h^2}u^*_{I-1,JK}-\frac{2D}{h^2}u^*_{IJK}+\frac{D}{h^2}u^*_{I+1,JK}, \\ \frac{1}{\Delta t}\left(u^*_{IJK}-u^n_{IJK}\right) &= \frac{D}{h^2}\left[(u^*_{I-1,JK}-u^*_{IJK})+(u^*_{I+1,JK}-u^*_{IJK})\right] \ge 0. \end{aligned}$$

According to the assumption, $u^n_{IJK} \ge 0$, and therefore we obtain $u^*_{IJK} \ge 0$. Next, Eq. (16) when $I = 1$ is given as following using the zero Neumann boundary condition:

$$\begin{aligned}\left(\frac{1}{\Delta t}+\frac{D}{h^2}\right)u^*_{1jk}-\frac{D}{h^2}u^*_{2jk} &= \frac{u^n_{1jk}}{\Delta t}, \\ \frac{1}{\Delta t}u^*_{1JK}-\frac{u^n_{1JK}}{\Delta t} &= \frac{D}{h^2}u^*_{2JK}-\frac{D}{h^2}u^*_{1JK}, \\ \frac{1}{\Delta t}\left(u^*_{1JK}-u^n_{1JK}\right) &= \frac{D}{h^2}\left(u^*_{2JK}-u^*_{1JK}\right). \end{aligned}$$

We can see that $u^*_{IJK} \ge 0$ also holds when $I = 1$. The case of $I = N_x$ can be proved similarly. Three cases imply that the minimum solution is positive, therefore $u^*_{ijk} \ge 0$ holds for all i, j and k. Proof for the y and z-direction OSM is done similarly, i.e., $u^{**}_{ijk} \ge 0$ and $u^{***}_{ijk} \ge 0$ for all i, j and k. The solution of the OSM holds positivity preserving. Positivity preserving for the interpolation method is shown in the same way as proving the discrete maximum principle. Recall that $\Phi_s, \Phi_{s+1} \in [0, 1]$ for all $s = 1, \dots, M$.

$$\begin{aligned}u^{n+1}_{ijk} &= \frac{I_{s+1}-u^{***}_{ijk}}{I_{s+1}-I_s}\Phi_s+\frac{u^{***}_{ijk}-I_s}{I_{s+1}-I_s}\Phi_{s+1} \\ &\ge \frac{I_{s+1}-u^{***}_{ijk}}{I_{s+1}-I_s}\times 0+\frac{u^{***}_{ijk}-I_s}{I_{s+1}-I_s}\times 0 = 0. \end{aligned}$$

This concludes the proof for the positivity preserving of the proposed numerical method.

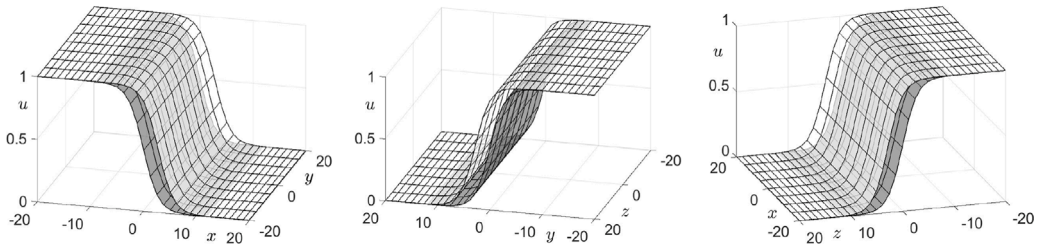

Fig. 3. From left to right, represent x–y, y–z and z–x direction. The initial condition and numerical solution is illustrated in gray and white, respectively.

Table 1
Temporal errors and convergence rates with an analytic solution.

Case	$\Delta_t = 0.5/4$	Rate	$\Delta_t = 0.5/8$	Rate	$\Delta_t = 0.5/16$	Rate	$\Delta_t = 0.5/32$
l_2-error	1.76×10^{-1}	0.99	8.88×10^{-2}	0.98	4.51×10^{-2}	0.95	2.33×10^{-2}

Table 2
Spatial errors and convergence rates with an analytic solution.

Case	$h = 40/32$	Rate	$h = 40/64$	Rate	$h = 40/128$	Rate	$h = 40/256$
l_2-error	1.11×10^{-1}	1.98	2.81×10^{-2}	1.98	7.14×10^{-3}	1.92	1.89×10^{-3}

5. Numerical experiments

In this section, we verify the convergence rate and unconditional stability of the proposed method, observe the effect of the diffusion coefficient and the order of the nonlinear term. Then, numerical examples using step functions and traveling waves are presented. Each of these is explored through numerical simulations. Unless otherwise stated, we applied the zero Neumann boundary condition for each numerical test and the coefficient K_{pq} is defined by Eq. (5).

5.1. Convergence test

The convergence rates in time and space are shown numerically using the following initial condition:

$$u(x, y, z, 0) = \frac{1}{1 + e^{x/\sqrt{2}}}, \tag{17}$$

with the following exact solution [41]:

$$u^{\text{ext}}(x, y, z, t) = \frac{1}{1 + e^{x/\sqrt{2} - t/2}}, \tag{18}$$

in domain $\Omega = (-20,\ 20) \times (-20,\ 20) \times (-20,\ 20)$ with $D = K_{pq} = 1$, $p = 2$ and $q = 1$. According to the discretization of the diffusion, we expect first-order convergence in time and second-order convergence in space. Fig. 3 illustrates the figure at times 0 and 4 in all three directions.

First, we set final time $T = 0.5$, number of space steps, $N_x = N_y = N_z = 256$ and apply a set of increasing time steps $N_t = 4,\ 8,\ 16$ and 32 to obtain the convergence rate for time. The error under a particular time step is defined as the l_2-norm of the difference between the analytic solution and the numerical solution. The corresponding convergence rate is defined by two l_2-norm errors with decreasing time steps.

$$e_{\Delta t} = \|u_{ijk} - u^{\text{ext}}_{ijk}\|_2,\ \text{convergence rate} = \log_2\left(\|e_{\Delta t}\|_2 / \|e_{\Delta t/2}\|_2\right) \tag{19}$$

The convergence rate for space is defined similarly. Table 1 lists resulting l_2-norm errors and corresponding convergence rates. We can find that the numerical scheme is first-order convergence in time.

Next, we set final time $T = 0.5$, number of time steps $N_t = 4096$ and apply a set of increasing space steps $N_x = N_y = N_z = 32,\ 64,\ 128$ and 256 with corresponding space step size $h = 40/N_x = 40/N_y = 40/N_z$ to obtain the convergence rate for space. Table 2 lists resulting l_2-norm errors and corresponding convergence rates. We can find that the numerical scheme is second-order convergence in space.

In general, the Fisher–KPP equation does not have an analytic solution. The previous convergence test considered a special case with an analytic solution. To highlight the versatility of the proposed method, we consider the case of $p = 1$ and $q = 9$ which the analytic solution does not exist under the authors' knowledge. Initial condition, computational domain and final time remain unchanged. $N_x = N_y = N_z = 256$ and $N_t = 4096$ is used for temporal and spatial convergence tests, respectively. We chose reference solutions u^{ref} for time and space convergence rates using small time step and space step size, respectively. The time reference solution for time convergence at final time T is obtained with $N_t = 256$. The same number of time steps, $N_t = 4,\ 8,\ 16$ and 32 are applied to

Table 3
Temporal errors and convergence rates with a reference solution.

Case	$\Delta_t = 0.5/4$	Rate	$\Delta_t = 0.5/8$	Rate	$\Delta_t = 0.5/16$	Rate	$\Delta_t = 0.5/32$
l_2-error	4.86×10^{-2}	0.99	2.46×10^{-2}	1.03	1.20×10^{-2}	1.09	5.66×10^{-3}

Table 4
Spatial errors and convergence rates with a reference solution.

Case	$h = 40/16$	Rate	$h = 40/32$	Rate	$h = 40/64$
l_2-error	4.17×10^{-1}	2.19	9.12×10^{-2}	1.90	2.44×10^{-2}

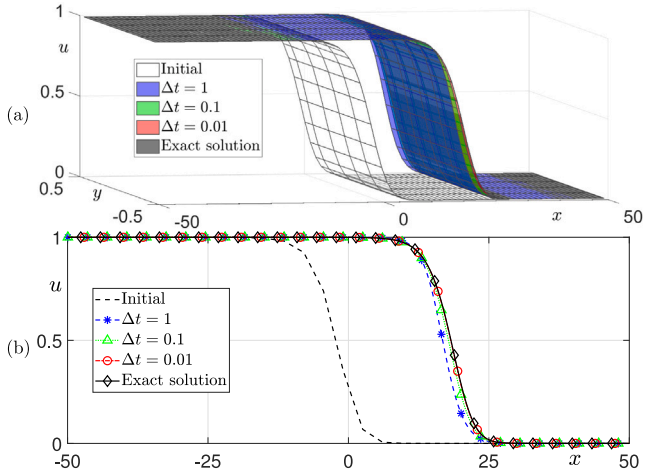

Fig. 4. Numerical solutions using $\Delta t = 1,\ 0.1,\ 0.01$ and exact solution when (a)$z = 0.05$ and (b) $y = z = 0.05$.

Table 5
Error when applying different time steps.

Time step	1	0.1	0.01
l_2-error	0.4039	0.1243	0.0131

calculate the convergence rate for time. The l_2-norm error is defined based on the reference solution, instead of the exact solution. Table 3 lists resulting l_2-norm errors and corresponding convergence rates. We can find that first-order convergence in time still holds.

The reference solution for space convergence at final time T is obtained with $N_x = N_y = N_z = 512$. l_2-norm errors when $N_x = N_y = N_z = 16,\ 32$ and 64 based on the reference solution using interpolation is defined in the following way:

$$e_h = \left\| u_{ijk} - \frac{1}{8} \sum_{a,b,c \in \{0,1\}} u^{\text{ref}}_{2^p i - 2^{p-1} + a, 2^p j - 2^{p-1} + b, 2^p k - 2^{p-1} + c} \right\|_2,$$

where $p = 3,\ 4$ and 5 with respect to $N_x = 64,\ 32$ and 16, respectively. Table 4 lists resulting l_2-norm errors and corresponding convergence rates. We can find that second-order convergence in space still holds.

5.2. Stability test

The unconditional stability can be demonstrated by applying large time steps for the proposed method. For the initial condition (17), the computational grid is given as $\Omega = (-50, 50) \times (-0.5, 0.5) \times (-0.5, 0.5)$ with parameters $N_x = 1000$, $N_y = N_z = 10$, $p = q = 1$, $D = K_{pq} = 1$ and final time $T = 10$ are used. Tests have been performed on three different time steps $\Delta t = 1, 0.1, 0.01$ which includes a exceptionally large time step $\Delta t = 1$. For each test, we calculated the l_2-norm error which is defined in Eq. (19). The results are given in Fig. 4(a) when $z = 0.05$ and Fig. 4(b) when $y = z = 0.05$. Large time step such as $\Delta t = 1$ is used, albeit the solution did not blow up. The error is given at Table 5. We can see that the numerical solutions did not blow up and agree with the exact solution when a sufficiently small time step is given.

5.3. Maximum principle and positive preserving

In this section, we revisit the maximum principle and positive preserving through numerical simulations. On the computational grid $\Omega = (0, 1) \times (0, 1) \times (0, 1)$ and $N_x = N_y = N_z = 64$ with parameters $D = p = q = 1$, we apply a randomly perturbed initial

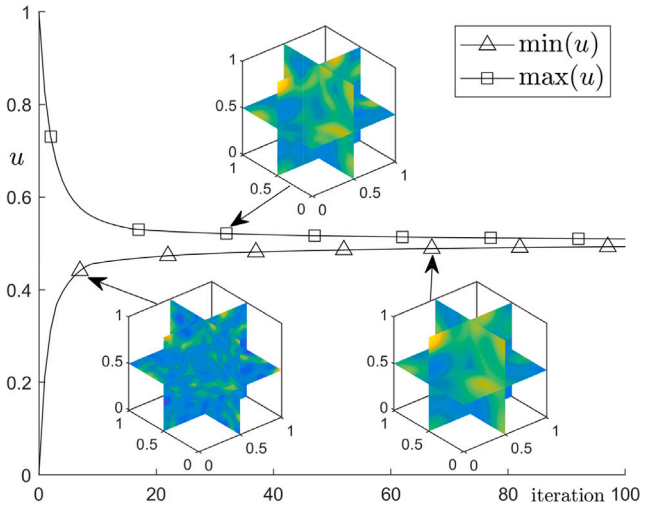

Fig. 5. Snapshot images of slice planes and temporal evolution of the maximum and minimum value.

condition where all values are in $[0, 1]$. Computational simulation is performed with time step $\Delta t = 10^{-4}$ until final time $T = 0.01$. Fig. 5 contains snapshot images of slice planes and temporal evolution of the maximum and minimum value of u^n_{ijk}, which confirms that the proposed method preserves positivity and maximum principle.

5.4. Effect of the diffusion coefficient

We performed computational experiments to validate the effect of diffusion coefficient D using the following initial condition.

$$u(x, y, z, 0) = 0.2\cos(2\pi x)\cos(2\pi y)\cos(2\pi z) + 0.5, \tag{20}$$

where $T = 0.06$, $\Delta t = 0.005$, $N_x = N_y = N_z = 64$ and $p = q = 1$ on domain $\Omega = (0,\ 1) \times (0,\ 1) \times (0,\ 1)$. Figs. 6 and 7 show the effect of diffusion coefficient D by illustrating the isosurfaces of level 0.5 and 0.6, respectively. At the top, the initial condition $u(x, y, z, 0)$ and the evolution of the total mass are given. From top to bottom indicates $D = 0.001$, $D = 0.01$, $D = 0.1$ and from left to right indicates $t = 0.02$, $t = 0.04$, $t = 0.06$. Comparing Figs. 6 and 7 we can obtain two conclusions: the total mass increases as time progresses, and it is roughly independent to D. However, the isosurface of level 0.5 varies depending on the value of D. Therefore, the coefficient D only affects the speed of diffusion and has none or little effect on the total mass.

The correlation between D and the total mass can be explained using the divergence theorem. Using the zero Neumann boundary condition, $\Delta u = 0$ for all t. Therefore, the total mass does not change when solving the diffusion Eq. (10). The total mass evolution illustrated in Fig. 6(b) will depend on Eq. (11), i.e., orders of nonlinear term.

Additionally, we can observe that the impact of different D values is more apparent in Fig. 6 (isosurface of level 0.5) than Fig. 7 (isosurface of level 0.6). In this numerical test, the diffusion equation varied by the value of D and the nonlinear equation was unchanged. We can conclude that the diffusion equation is more dominant than the nonlinear equation at $u = 0.5$. Therefore D has a significant impact on the evolution dynamics. However, when $u = 0.6$, the nonlinear equation is dominant, making D have a minor impact.

5.5. Orders of nonlinear term

As described in Section 1, orders of nonlinear term p and q significantly affect the dynamics of the modified Fisher–KPP equation. According to the last section, we expect values of p and q to have a major impact on the evolution of the total mass. In order to focus on the evolutionary difference between different values of p and q, the following initial condition

$$u(x, y, z, 0) = 0.45\cos(2\pi x)\cos(2\pi y)\cos(2\pi z) + 0.5, \tag{21}$$

is applied on domain $\Omega = (0,\ 1) \times (0,\ 1) \times (0,\ 1)$ with $D = 0.001$. Unless otherwise stated, we use $N_x = N_y = N_z = 256$ and $\Delta t = 0.01$ for this section. Note that we minimized the diffusion term and emphasized the nonlinear reaction term by applying a small value of D. First we consider the case when p and q are equal, then study the case when they are different.

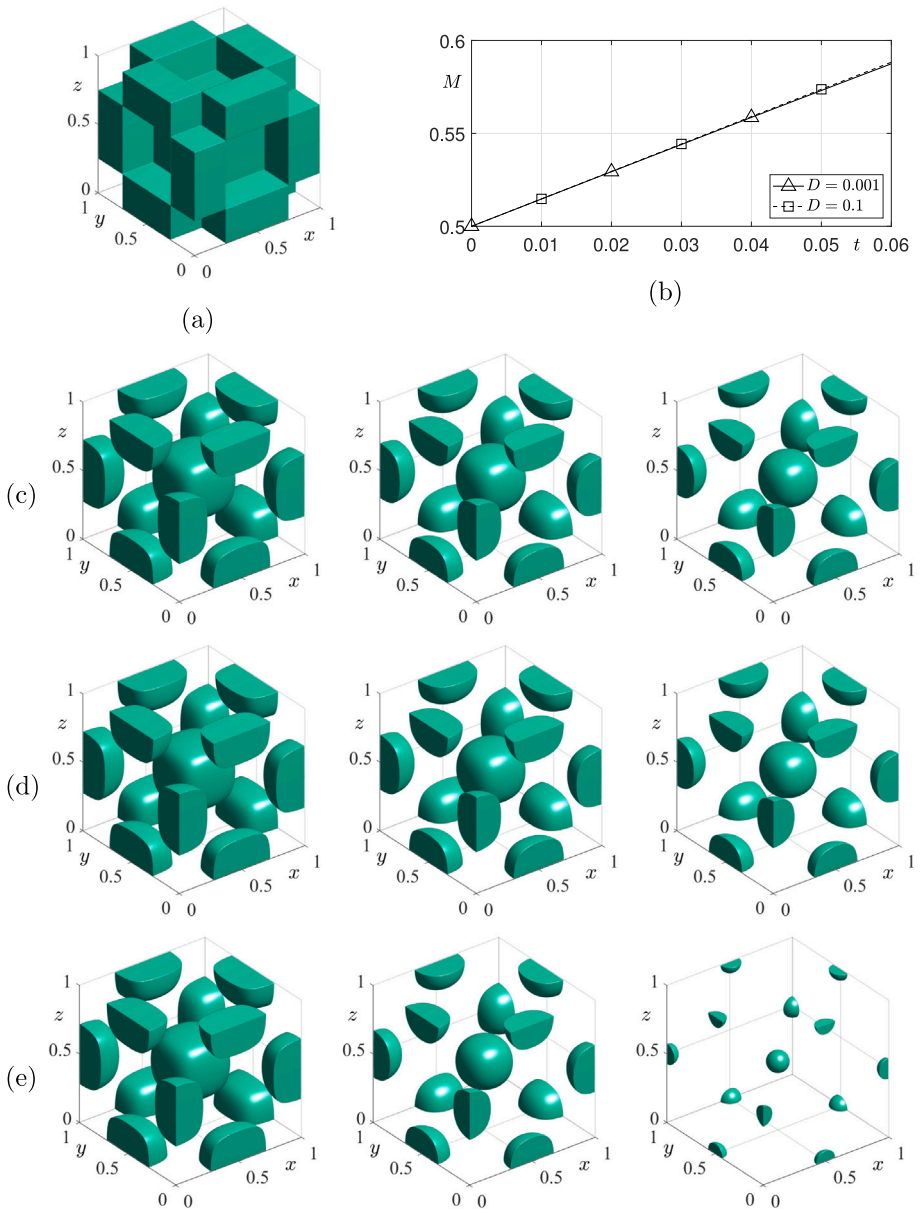

Fig. 6. Effect of D demonstrated by isosurfaces of level 0.5. Evolution of initial condition (a) at different conditions (c) $D = 0.001$, (d) $D = 0.01$ and (e) $D = 0.1$ observed below. (b) illustrates the total mass of numerical results.

5.5.1. Nonlinear term with same order

We must mention the variations of $K_{pq}u^p(1-u)^q$ with different parameter values. As shown in Fig. 8, the maximum value is reached at $u = 0.5$.

We first demonstrate when p and q have same values. Orders $p = q = 1$ and $p = q = 10$ are applied until final time $T = 0.4$. Fig. 9 illustrates isosurfaces of the numerical results. Fig. 9(a) is the isosurface of initial condition at level 0.5 and Fig. 9(b) is the isosurface of initial condition at level 0.7. Fig. 9(c) shows the evolution of the total mass for $p = q = 1$ and $p = q = 10$, where the total mass for $p = q = 1$ overtakes the total mass of $p = q = 10$. Fig. 9(d) and (e) are the isosurfaces of $p = q = 1$ at level 0.5 and 0.7, respectively. Fig. 9(f) and (g) are the isosurfaces when $p = q = 10$ at level 0.5 and 0.7, respectively. Evolutionary snapshots are listed in the order of $t = 0.1$, $t = 0.2$ and $t = 0.4$. The overtake of total mass can be explained through Fig. 8. The diffusion equation has the mass conservation property. Therefore we focus on the nonlinear equation. In Fig. 8, $K_{pq}u^p(1-u)^q$ of $p = q = 1$ is overtaken by $K_{pq}u^p(1-u)^q$ of $p = q = 10$ as u increases from 0.5 to 1. Therefore, when total mass increases from 0.5 to 1, $K_{pq}u^p(1-u)^q$ of $p = q = 10$ will tend to be larger than $p = q = 1$, causing an overtake in total mass. This phenomenon can also be observed through isosurfaces. We can see that the difference between Fig. 9(d) and (e) at $t = 0.4$ is much larger than the difference between Fig. 9(f)

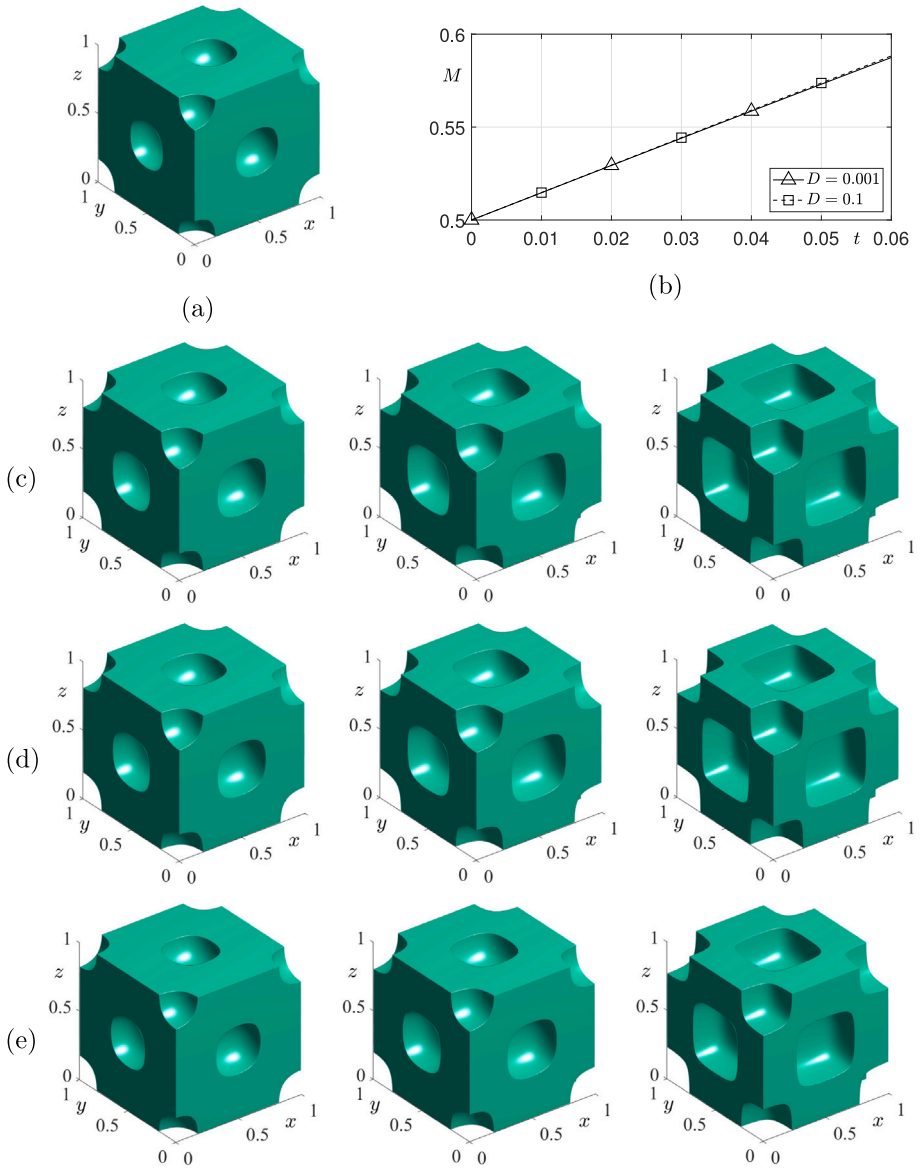

Fig. 7. Effect of D demonstrated by isosurfaces of level 0.6. Evolution of initial condition (a) at different conditions (c) $D = 0.001$, (d) $D = 0.01$ and (e) $D = 0.1$ at $t = 0.02, 0.04, 0.06$. (b) illustrates the evolution of total mass.

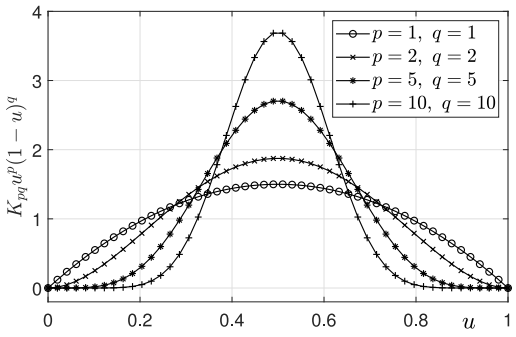

Fig. 8. Variations of $K_{pq}u^p(1-u)^q$ when $p = q = 1,\ 2,\ 5$, and 10.

and (g) at $t = 0.4$. Moreover, we can observe that the isosurfaces are small, which indicates that u_{ijk} in the computational domain is mostly large. Therefore, the isosurface results agree well with the overtake illustrated in Fig. 9(c).

Fig. 10 illustrates the subtraction $p = 10$ from $p = 1$ at $z = 0.5$ when $t = 0.1,\ 0.2$, and 0.4. The numerical result indicates that the small concentration of mass when $p = q = 1$ increases faster than in case of $p = q = 10$.

5.5.2. Nonlinear term with different order

We move on to the case when p and q have different values. Orders $(p,\ q) = (1,\ 9)$ and $(9,\ 1)$ are applied until final time $T = 0.6$. Fig. 11 illustrates isosurfaces of the numerical results. Fig. 11(a) is the isosurface of initial condition at level 0.5 and Fig. 11(b) is the isosurface of initial condition at level 0.7. Fig. 11(c) shows the evolution of the total mass for $(p,\ q) = (1,\ 9),\ (9,\ 1)$, where the total mass for $(p,\ q) = (1,\ 9)$ becomes dominant than $(p,\ q) = (1,\ 9)$. Fig. 11(d) and (e) are the isosurfaces of $(p,\ q) = (1,\ 9)$ at levels 0.5 and 0.7, respectively. Fig. 11(f) and (g) are the isosurfaces when $(p,\ q) = (9,\ 1)$ at level 0.5 and 0.7, respectively. Evolutionary snapshots are listed in the order of $t = 0.2$, $t = 0.4$ and $t = 0.6$. The discussion of the total mass when $p \neq q$ starts with considering the nonlinear term, since the diffusion equation has the mass conservation property. The nonlinear term is $u^9(1-u)$ when $(p,\ q) = (9,\ 1)$, and $u(1-u)^9$ when $(p,\ q) = (1,\ 9)$. All other conditions are the same, including the coefficient K. Therefore we subtract two nonlinear terms:

$$u^9(1-u) - u(1-u)^9 = u(1-u)[u^8 - (1-u)^7]. \tag{22}$$

Eq. (22) is positive when $u > 0.5$ and negative when $u < 0.5$. Therefore, we can assume that the total mass for $(p,\ q) = (9,\ 1)$ will increase faster than the total mass of $(p,\ q) = (1,\ 9)$ when the majority of u is over 0.5. The total mass difference between $(p,\ q) = (9,\ 1)$ and $(p,\ q) = (1,\ 9)$ will become larger overtime because the total mass increases and more u_{ijk} will be over 0.5. This describes the dominant total mass for $(p,\ q) = (9,\ 1)$ compared to $(p,\ q) = (1,\ 9)$ shown in Fig. 11(c). The total mass can also be demonstrated through isosurfaces. First, isosurfaces of level 0.5 (Fig. 11(d) and (f)) are not considerably small nor large. However, when $(p,\ q) = (1,\ 9)$, the isosurface of level 0.7 (Fig. 11(e)) is considerably large, which indicates that on the computational domain, there are less u_{ijk} that is over the value of 0.7. On the other hand, when $(p,\ q) = (9,\ 1)$, the isosurface of level 0.7 (Fig. 11(e)) is similar to the isosurface of level 0.5. This indicates that there are more u_{ijk} that is over the value of 0.7. We can conclude that when $(p,\ q) = (1,\ 9)$, value of u_{ijk} is mostly between 0.5 and 0.7, whereas when $(p,\ q) = (9,\ 1)$, many u_{ijk} are over 0.7. Therefore, the total mass is larger when $(p,\ q) = (9,\ 1)$, which agrees well with the result in Fig. 11(c).

5.6. Evolution of step functions

The practicability of the proposed numerical method is demonstrated through numerical simulations. We start with a series of step functions defined in $\Omega = (-1.2,\ 1.2) \times (-1.2,\ 1.2) \times (-1.2,\ 1.2)$ with space steps $N_x = N_y = N_z = 120$ that have the same total mass at the initial state. We set the following initial conditions:

$$u(x,y,z,0) = \begin{cases} 0.2, & \text{if } -0.57 \le x \le 0.61, \\ 0, & \text{otherwise.} \end{cases} \tag{23}$$

$$u(x,y,z,0) = \begin{cases} 0.2, & \text{if } -0.97 + 0.8k \le x \le -0.59 + 0.8k \text{ for } k = 0,\ 1,\ 2, \\ 0, & \text{otherwise.} \end{cases} \tag{24}$$

$$u(x,y,z,0) = \begin{cases} 0.2, & \text{if } -1.07 + 0.4k \le x \le -0.89 + 0.4k \text{ for } k = 0, \dots, 5, \\ 0, & \text{otherwise.} \end{cases} \tag{25}$$

Diffusion coefficient is set as $D = 0.05$ and identical p and q values are selected: $p = q = 5$. Fig. 12 illustrates the numerical simulations of step functions until final time $T = 1.2$ using time step $\Delta t = 0.01$. Evolutionary snapshots at $t = 0,\ 40\Delta t,\ 80\Delta t$ and $120\Delta t$ of Eqs. (23)–(25) are illustrated in Fig. 12(a)–(c), respectively. Temporal evolution of the total mass for each case is given in Fig. 12(d). We can find the overtake of the total mass between the first case and the second case, whereas the third case remained smaller than the others. Albeit having the same total mass, evolution can vary among different step functions.

5.7. Traveling wave solution

Traveling waves are widely studied form for reaction–diffusion equation. due to important applications to biology and chemistry. The Fisher–KPP equation is the first to study the solution of the traveling waves. We perform simulations with traveling wave for different values of p and q. The computational domain is given as $\Omega = (-20,\ 80) \times (-2,\ 2) \times (-2,\ 2)$ with $N_x = 500$, $N_y = 20$, $N_z = 20$. The diffusion coefficient and time step is given as $\Delta t = 0.01$ and $D = 1$, respectively. We apply the following initial condition with $(p,\ q) = (1,\ 1),\ (1.1,\ 1.1),\ (2,\ 2)$:

$$u(x,y,z,0) = \left[\frac{1}{2} - \frac{1}{2}\tanh\left(\frac{x}{2\sqrt{6}}\right)\right]^2.$$

Results at $t = 8$ are illustrated in Fig. 13. There are two discussions. First is that the initial condition traveled a short distance when large p and q are applied. Second, the thickness of the transition layer decreases for larger p and q values. The thickness can be explained from Fig. 8, where the overall profile of the nonlinear reaction term becomes narrower for larger p and q values.

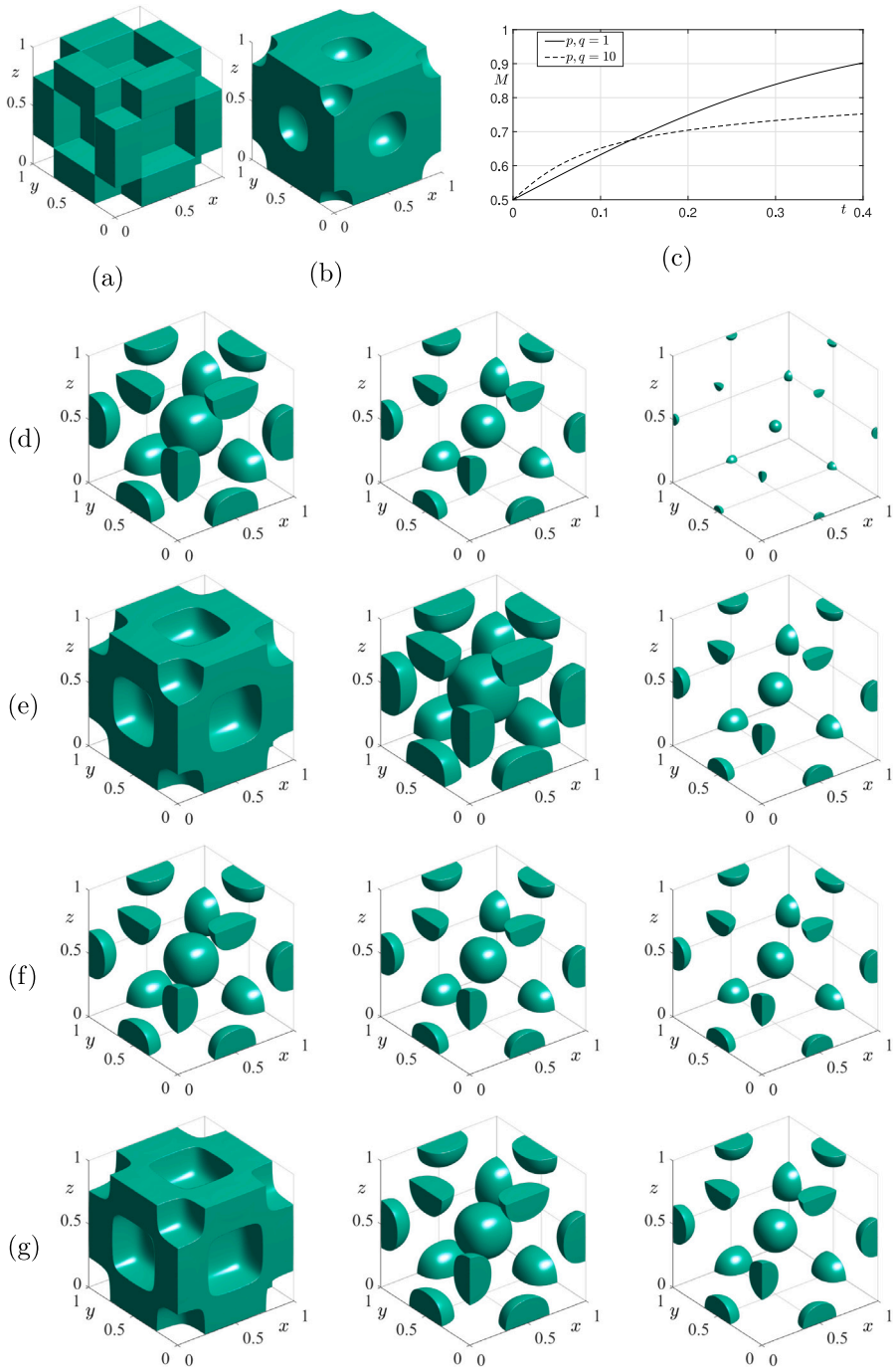

Fig. 9. Demonstration of evolution dynamics when $p = q$ with snapshots at $t = 0.1, 0.2, 0.4$. (a) Initial solution, (d) $p = q = 1$ and (f) $p = q = 10$ illustrated in isosurface level 0.5. (b) Initial solution, (e) $p = q = 1$ and (g) $p = q = 10$ illustrated in isosurface level 0.7. (c) illustrates the evolution of total mass.

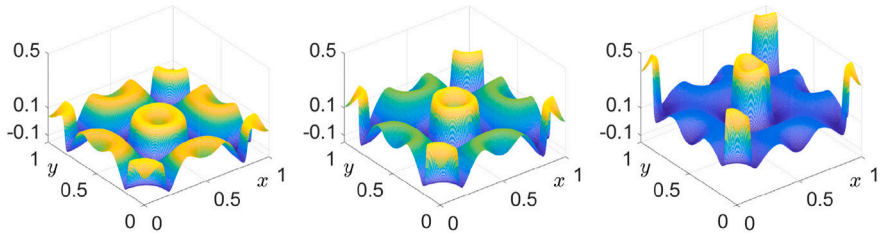

Fig. 10. Subtraction $p = 10$ from $p = 1$ at $z = 0.5$ when $t = 0.1, 0.2$, and 0.4.

6. Conclusions

The main result of the present work is the novel numerical method for solving the three-dimensional modified Fisher–KPP equation in 3D. After splitting the modified Fisher–KPP equation, the diffusion term and nonlinear term are solved using the OSM and interpolation method, respectively. Analytic studies showed that the numerical solution is bounded by the discrete maximum principle and positivity preserving. Numerical simulations demonstrated the unconditional stability by applying various time step sizes and the numerical algorithm did not blow up. Following numerical tests showed that the proposed method is first-order convergence in time and second-order convergence in space. The effects of the diffusion coefficient and orders of the nonlinear term is studied using the total mass. Evolution of benchmark problems such as step functions and traveling wave demonstrated the practicability of the proposed method.

Data availability

No data was used for the research described in the article.

Use of AI tools declaration

The authors declare they have not used Artificial Intelligence (AI) tools in the creation of this article.

Acknowledgments

The corresponding author (J.S. Kim) was supported by the Brain Korea 21 FOUR from the Ministry of Education of Korea. The authors thank the reviewers for their constructive and helpful comments on the revision of this article.

Appendix A. Algorithm OSM

We express Eqs. (7)–(9) in an implicit form as following:

$$\alpha u^{*}_{i-1,j,k} + \beta u^{*}_{ijk} + \gamma u^{*}_{i+1,j,k} = f^{n}_{ijk}, \tag{26}$$

$$\alpha u^{**}_{i,j-1,k} + \beta u^{**}_{ijk} + \gamma u^{**}_{i,j+1,k} = g^{*}_{ijk}, \tag{27}$$

$$\alpha u^{***}_{i,j,k-1} + \beta u^{***}_{ijk} + \gamma u^{***}_{i,j,k+1} = h^{**}_{ijk}, \tag{28}$$

where

$$\alpha = -\frac{D}{h^2},\ \beta = \frac{1}{\Delta t} + \frac{2D}{h^2},\ \gamma = -\frac{D}{h^2},\ f^{n}_{ijk} = \frac{u^{n}_{ijk}}{\Delta t},\ g^{*}_{ijk} = \frac{u^{*}_{ijk}}{\Delta t},\ h^{**}_{ijk} = \frac{u^{**}_{ijk}}{\Delta t}.$$

Consider Eqs. (26), (27) and (28) in the system of index i, j and k, respectively and we obtain the following tridiagonal systems:

$$A u^{*}_{1:N_x,j,k} = f^{n}_{1:N_x,j,k}, \tag{29}$$

$$A u^{**}_{i,1:N_y,k} = g^{*}_{i,1:N_y,k}, \tag{30}$$

$$A u^{***}_{i,j,1:N_z} = h^{**}_{i,j,1:N_z}. \tag{31}$$

Here, $u^{*}_{1:N_x,j,k}, u^{**}_{i,1:N_y,k}$ and $u^{***}_{i,j,1:N_z}$ is the solution vector and the coefficient matrix is given as

$$A = \begin{pmatrix} \beta+\alpha & \gamma & 0 & \dots & 0 & 0 \\ \alpha & \beta & \gamma & \dots & 0 & 0 \\ 0 & \alpha & \beta & \dots & 0 & 0 \\ \vdots & \vdots & \ddots & \ddots & \ddots & \vdots \\ 0 & 0 & 0 & \dots & \beta & \gamma \\ 0 & 0 & 0 & \dots & \alpha & \beta+\gamma \end{pmatrix}. \tag{32}$$

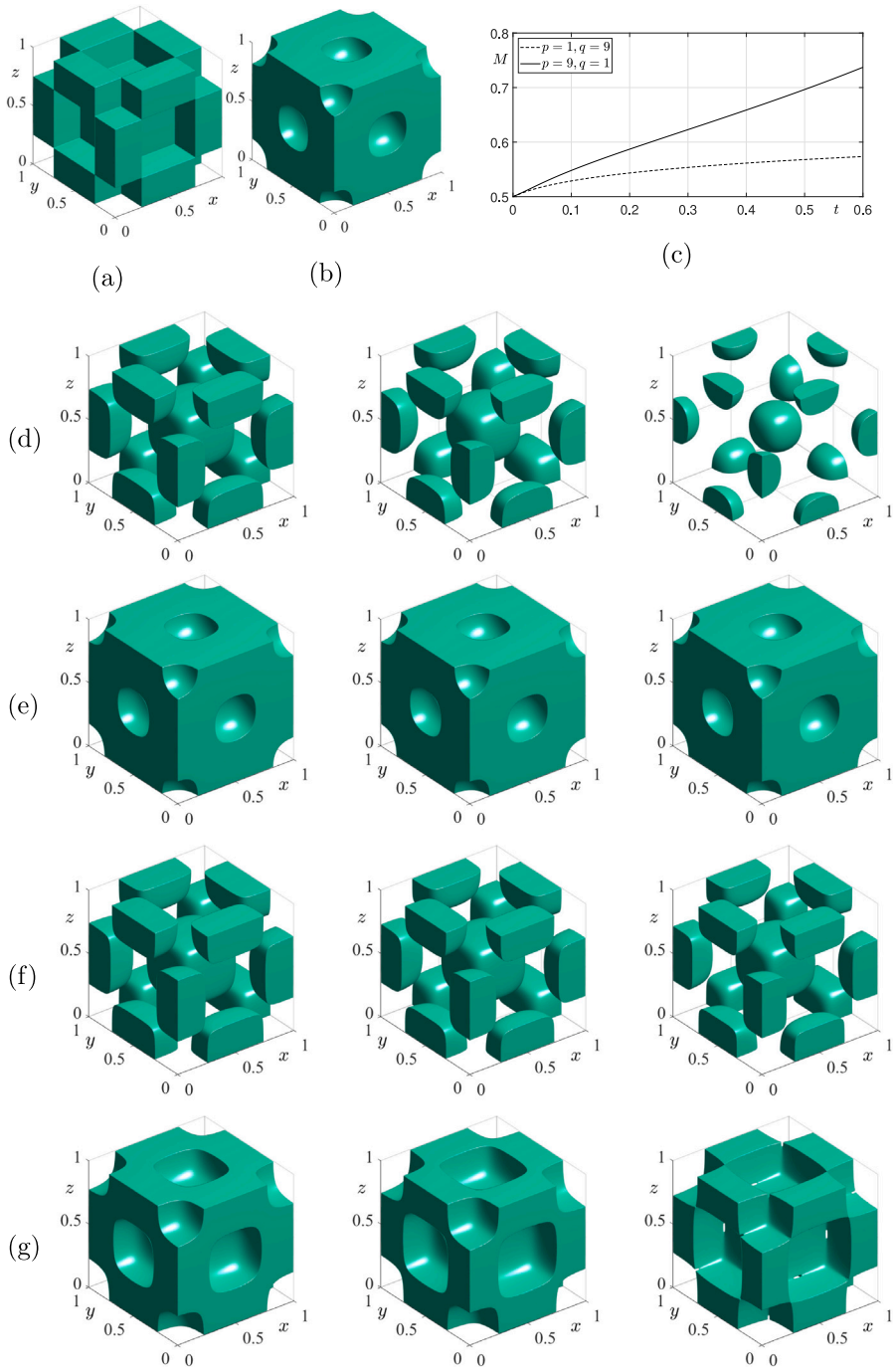

Fig. 11. Demonstration of evolution dynamics when $p = q$ with snapshots at $t = 0.2, 0.4, 0.6$. (a) Initial solution, (d) $(p, q) = (1, 9)$ and (f) $(p, q) = (9, 1)$ illustrated in isosurface level 0.5. (b) Initial solution, (e) $(p, q) = (1, 9)$ and (g) $(p, q) = (9, 1)$ illustrated in isosurface level 0.7. (c) illustrates the evolution of total mass.

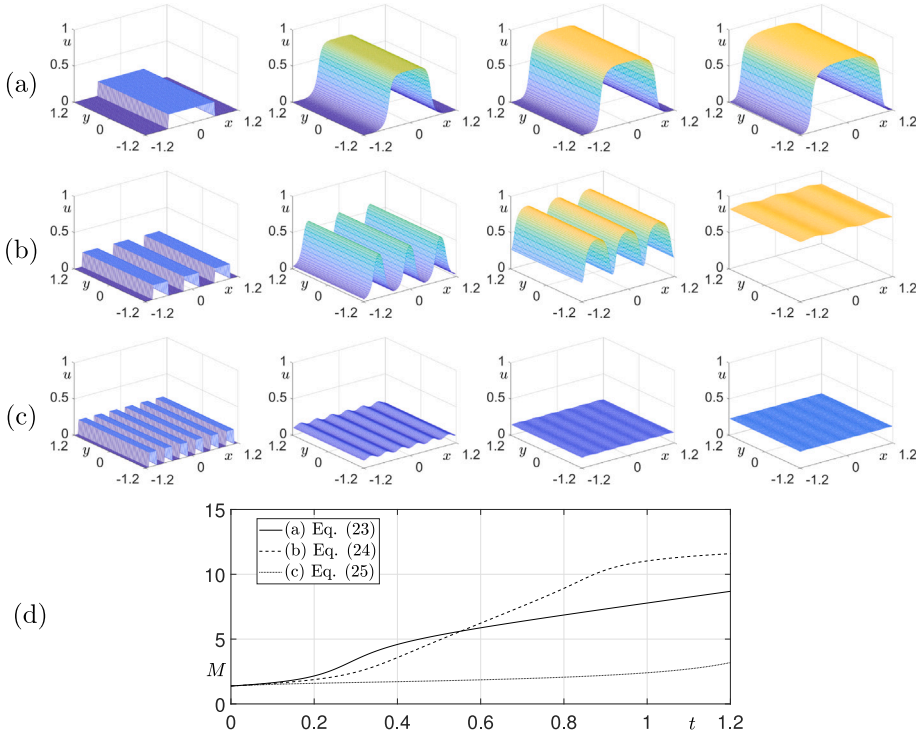

Fig. 12. Evolution of step functions at $t = 0$, $40\Delta t$, $80\Delta t$ and $120\Delta t$ for (a) Eq. (23), (b) Eq. (24) and (c) Eq. (25). The total mass for each case is drawn at (d).

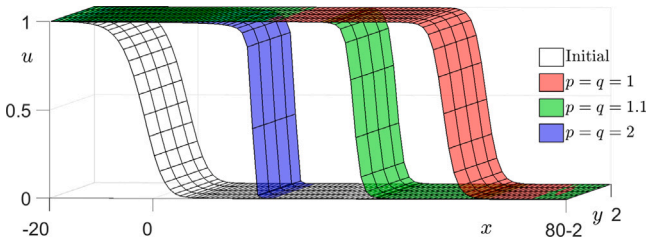

Fig. 13. Numerical solutions of the traveling wave at $t = 8$ for $(p,\ q) = (1,\ 1),\ (1.1,\ 1.1),\ (2,\ 2)$.

Each tridiagonal systems are solved using the Thomas algorithm. The following equation illustrates the solution for Eq. (26). The other equations can be derived similarly.

for $j = 1 : N_y$
  for $k = 1 : N_z$
    for $i = 1 : N_x$
      Set f^n_{ijk} by Eq. (29)
    end
    Solve $Au^*_{1:N_x,j,k} = f^n_{1:N_x,j,k}$
  end
end

Appendix B. Pseudo code

Algorithm 1 Numerical scheme for the 3D Fisher–KPP equation

Input: endpoints $L_x,\ R_x,\ L_y,\ R_y,\ L_z,\ R_z$; number of grids $N_x,\ N_y,\ N_z$; initial condition u^0; final time T; time step size Δt; parameters $p,\ q,\ D,\ K$; number of pre-computing grids M
Output: approximation of $u(x,\ y,\ z,\ T)$
Step 1: Initialization
  $N_t = T/\Delta t,\ h = (R_x - L_x)/N_x$ and $n = 0$
  for $i = 1, \cdots, N_x,\ j = 1, \cdots, N_y,\ k = 1, \cdots, N_z$ **do**
    $x_i = L_x + (i - 0.5)h$
    $y_j = L_y + (j - 0.5)h$
    $z_k = L_z + (k - 0.5)h$
    $u^0_{ijk} = u^0_{ijk}$
  end for
Step 2: Pre-computing
  $\alpha = -D/h^2,\ \beta = 1/\Delta t + 2D\ h^2,\ \gamma = -D/h^2$
  Calculate A (Eq. (32))
  for $s = 1, \cdots, M$ **do**
    $I_s = (s - 1)/(M - 1)$
    Calculate N_τ (Eq. (12))
    Calculate Φ ([36])
  end for
Step 3: Main algorithm
  for $n = 0, \cdots N_t - 1$ **do Steps 4-7**
    Step 4: Equation (7)
      Apply zero Neumann boundary condition
      for $j = 1, \cdots, N_y,\ k = 1, \cdots, N_z$ **do**
        for $i = 1, \cdots, N_x$ **do**
          $f_{ijk} = u^n_{ijk}/\Delta t$
        end for
        Solve $Au^*_{1:N_x,j,k} = f^n_{1:N_x,j,k}$ (Thomas algorithm)
      end for
    Step 5: Solve equation (8)
      Apply zero Neumann boundary condition
      for $i = 1, \cdots, N_x,\ k = 1, \cdots, N_z$ **do**
        for $j = 1, \cdots, N_y$ **do**
          $g^*_{ijk} = u^*_{ijk}/\Delta t$
        end for
        Solve $Au^{**}_{i,1:N_y,k} = g^*_{i,1:N_y,k}$ (Thomas algorithm)
      end for
    Step 6: Solve equation (9)
      Apply zero Neumann boundary condition
      for $i = 1, \cdots, N_x,\ j = 1, \cdots, N_y$ **do**
        for $ks = 1, \cdots, N_z$ **do**
          $h^{**}_{ijk} = u^{**}_{ijk}/\Delta t$
        end for
        Solve $Au^{***}_{i,j,1:N_z} = h^{**}_{i,j,1:N_z}$ (Thomas algorithm)
      end for
    Step 7: Solve equation (11)
      for $i = 1, \cdots, N_x,\ j = 1, \cdots, N_y,\ k = 1, \cdots, N_z$ **do**
        Set s such that $I_s \le u^{***}_{ijk} \le I_{s+1}$
        $u^{n+1}_{ijk} = (I_{s+1} - u^{***}_{ijk})/(I_{s+1} - I_s)\Phi_s + (u^{***}_{ijk} - I_s)/(I_{s+1} - I_s)\Phi_{s+1}$
      end for
  end for
return $u(x_i,\ y_j,\ z_k, N_t\Delta t)$

References

[1] R.A. Fisher, The wave of advance of advantageous genes, Ann. Eugen. 7 (4) (1937) 355–369.
[2] A. Kolmogorov, N. Petrovsky, N. Piskunov, Etude de l'équation de la diffusion avec croissance de la quantité de matière et son application à un probléme biologique, Moscow Univ. Math. Bull. 1 (1937) 1–25.
[3] S. Penington, The spreading speed of solutions of the non-local Fisher–KPP equation, J. Funct. Anal. 275 (12) (2018) 3259–3302.
[4] B. Perthame, S. Génieys, Concentration in the nonlocal Fisher equation: the hamilton–Jacobi limit, Math. Model. Nat. Phenom. 2 (4) (2007) 135–151.
[5] H. Berestycki, G. Nadin, B. Perthame, L. Ryzhik, The non-local Fisher–KPP equation: travelling waves and steady states, Nonlinearity 22 (12) (2009) 2813.
[6] F. Hamel, C. Henderson, Propagation in a Fisher–KPP equation with non-local advection, J. Funct. Anal. 278 (7) (2020) 108426.
[7] F. Achleitner, C. Kuehn, On bounded positive stationary solutions for a nonlocal Fisher–KPP equation, Nonlinear Anal. 112 (2015) 15–29.
[8] A.V. Shapovalov, A.E. Kulagin, S.A. Siniukov, Pattern formation in a nonlocal Fisher–Kolmogorov–Petrovsky–Piskunov model and in a nonlocal model of the kinetics of an metal vapor active medium, Russian Phys. J. 65 (4) (2022) 695–702.
[9] A. Audrito, J.L. Vézquez, The Fisher–KPP problem with doubly nonlinear diffusion, J. Differential Equations 263 (11) (2017) 7647–7708.
[10] T. Xu, S. Ji, M. Mei, J. Yin, Critical sharp front for doubly nonlinear degenerate diffusion equations with time delay, Nonlinearity 35 (7) (2022) 3358.
[11] W. Qin, D. Ding, X. Ding, Two boundedness and monotonicity preserving methods for a generalized Fisher–KPP equation, Appl. Math. Comput. 252 (2015) 552–567.
[12] F. Wang, L. Xue, K. Zhao, X. Zheng, Global stabilization and boundary control of generalized Fisher/KPP equation and application to diffusive SIS model, J. Differential Equations 275 (2021) 391–417.
[13] J.E. Macías-Díaz, I.E. Medina-Ramírez, A. Puri, Numerical treatment of the spherically symmetric solutions of a generalized Fisher–Kolmogorov–Petrovsky–Piskunov equation, J. Comput. Appl. Math. 231 (2) (2009) 851–868.
[14] B.H. Gilding, R. Kersner, Travelling Waves in Nonlinear Diffusion Convection Reaction, vol. 60, Birkhauser, 2012.
[15] A.C. Newell, J.A. Whitehead, Finite bandwidth, finite amplitude convection, J. Fluid Mech. 38 (2) (1969) 279–303.
[16] R. FitzHugh, Impulses and physiological states in theoretical models of nerve membrane, Biophys. J. 1 (6) (1961) 445–466.
[17] J. Nagumo, S. Arimoto, S. Yoshizawa, An active pulse transmission line simulating nerve axon, Proc. IRE 50 (10) (1962) 2061–2070.
[18] J.M. Burgers, A mathematical model illustrating the theory of turbulence, Adv. Appl. Mech. 1 (1948) 171–199.
[19] J. Gärtner, Location of wave fronts for the multi-dimensional K–P–P Equation and Brownian first exit densities, Math. Nachr. 105 (1) (1982) 317–351.
[20] A. Ducrot, On the large time behaviour of the multi-dimensional Fisher–KPP equation with compactly supported initial data, Nonlinearity 28 (4) (2015) 1043.
[21] Y. Du, W. Ni, The high dimensional Fisher–KPP nonlocal diffusion equation with free boundary and radial symmetry, part 1, SIAM J. Math. Anal. 54 (3) (2022) 3930–3973.
[22] B. Lou, J. Lu, Spreading in a cone for the Fisher–KPP equation, J. Differential Equations 267 (12) (2019) 7064–7084.
[23] S. Vyas, M.D. Golub, D. Sussillo, K.V. Shenoy, Computation through neural population dynamics, Annu. Rev. Neurosci. 43 (2020) 249–275.
[24] G.A. Al-Musawi, A.J. Harfash, Finite element analysis of extended Fisher-Kolmogorov equation with Neumann boundary conditions, Appl. Numer. Math. 201 (2024) 41–71.
[25] C.M. Garvey, E. Spiller, D. Lindsay, C.T. Chiang, N.C. Choi, D.B. Agus, P. Mallick, J. Foo, S.M. Mumenthaler, A high-content image-based method for quantitatively studying context-dependent cell population dynamics, Sci. Rep. 6 (2016) 29752.
[26] D.G. Aronson, H.F. Weinberger, Multidimensional nonlinear diffusion arising in population genetics, Adv. Math. 30 (1) (1978) 33–76.
[27] V.P. Zhdanov, Proliferation of cells with aggregation and communication, Math. Biosci. 301 (2018) 32–36.
[28] Y. Du, H. Matsuzawa, M. Zhou, Spreading speed and profile for nonlinear Stefan problems in high space dimensions, J. Math. Pures Appl. 103 (3) (2015) 741–787.
[29] Y. Du, Z. Guo, Spreading-vanishing dichotomy in a diffusive logistic model with a free boundary, II, J. Differential Equations 250 (12) (2011) 4336–4366.
[30] S. MacNamara, G. Strang, Splitting Methods in Communication, Imaging, Sci. Eng, Springer, 2016, pp. 95–114.
[31] Q. Li, F. Song, Splitting spectral element method for fractional reaction–diffusion equations, J. Algorithms Comput. Technol. 14 (2020) 1748302620966705.
[32] J. Wang, Z. Han, W. Jiang, J. Kim, A fast, efficient, and explicit phase-field model for 3D mesh denoising, Appl. Math. Comput. 458 (2023) 128239.
[33] S. Ham, S. Kwak, C. Lee, G. Lee, J. Kim, A second-order time-accurate unconditionally stable method for a gradient flow for the Modica–Mortola functional, J. Sci. Comput. 95 (2) (2023) 63.
[34] S. Ham, J. Kim, Stability analysis for a maximum principle preserving explicit scheme of the Allen–Cahn equation, Math. Comput. Simulation 207 (2023) 453–465.
[35] S.D. Conte, C. de Boor, Elementary Numerical Analysis, McGraw-Hill, New York, 1965, p. 1972.
[36] S. Kim, C. Lee, H.G. Lee, H. Kim, S. Kwak, Y. Hwang, S. Kang, S. Ham, J. Kim, An unconditionally stable positivity-preserving scheme for the one-dimensional Fisher–Kolmogorov–Petrovsky–Piskunov equation, Discrete Dyn. Nat. Soc. 2021 (2021) 7300471.
[37] S. Bian, On the Fisher–KPP model with nonlocal nonlinear sources, Math. Nachr. 297 (1) (2024) 144–164.
[38] J.E. Macías-Díaz, A. Gallegos, On a positivity-preserving numerical model for a linearized hyperbolic Fisher–Kolmogorov–Petrovski–Piskunov equation, J. Comput. Appl. Math. 354 (2019) 603–611.
[39] R. Company, V.N. Egorova, L. Jódar, Conditional full stability of positivity-preserving finite difference scheme for diffusion–advection-reaction models, J. Comput. Appl. Math. 341 (2018) 157–168.
[40] R.S. Varga, On a discrete maximum principle, SIAM J. Numer. Anal. 3 (2) (1966) 355–359.
[41] G. Arora, V. Joshi, A computational approach for solution of one dimensional parabolic partial differential equation with application in biological processes, Ain Shams Eng. J. 9 (4) (2018) 1141–1150.